Dipolar Bose-Einstein condensates with dipole-dependent scattering length

Shai Ronen,[1] Daniele C. E. Bortolotti,[2] D. Blume,[3] and John L. Bohn[4,*]
[1]*JILA and Department of Physics, University of Colorado, Boulder, Colorado 80309-0440, USA*
[2]*LENS and Dipartimento di Fisica, Universitá di Firenze, and INFM, Sesto Fiorentino, Italy*
[3]*Department of Physics and Astronomy, Washington State University, Pullman, Washington 99164-2814, USA*
[4]*JILA, NIST and Department of Physics, University of Colorado, Boulder, Colorado 80309-0440, USA*
(Received 9 May 2006; published 19 September 2006)

We consider a Bose-Einstein condensate of polar molecules in a harmonic trap, where the effective dipole may be tuned by an external field. We demonstrate that taking into account the dependence of the scattering length on the dipole moment is essential to reproducing the correct energies and for predicting the stability of the condensate. We do this by comparing Gross-Pitaevskii calculations with diffusion Monte Carlo calculations. We find very good agreement between the results obtained by these two approaches once the dipole dependence of the scattering length is taken into account. We also examine the behavior of the condensate in nonisotropic traps.

DOI: 10.1103/PhysRevA.74.033611 PACS number(s): 03.75.Hh, 03.75.Nt

I. INTRODUCTION

Degenerate atomic quantum gases are typically very dilute systems. Nevertheless, inter-atomic interactions strongly determine many of the observed phenomena and their underlying physics [1,2]. Until recently, only short-range and isotropic interactions have been considered. However, recent developments in the manipulation of cold atoms and molecules have been paving the way towards the analyses of polar gases in which dipole-dipole interparticle interactions are important [3–8]. A major break through has been very recently achieved by the experimental group in Stuttgart [9], where a Bose-Einstein condensate (BEC) of strongly magnetic ^{52}Cr atoms has been realized. This experiment observed the effects of dipole-dipole interactions on the shape of the condensate. New exciting phenomena are expected to occur in these quantum gases since the particles interact via dipole-dipole interactions which are long ranged and anisotropic. Recent theoretical analyses have shown that the stability and excitations of dipolar gases are crucially determined by the trap geometry [10–18].

Yi and You [11,12] first introduced a pseudopotential appropriate for describing slowly moving particles interacting via short-range repulsive forces and long-range dipolar forces. The dipolar long-range part of their pseudopotential is identical to the long-range part of the original potential. The pseudopotential also includes a contact (δ function) potential whose coefficient is proportional to the scattering length. For nonpolar particles, the scattering length is solely due to short range interactions. A crucial point that Yi and You have shown is that the scattering length is also dependent on the long-range dipolar interaction. They have argued for the need to take this into account when calculating condensate properties through the Gross-Pitaevskii equation (GPE). However, they stopped short of actually explicitly showing how condensate properties are influenced by the dependence of the scattering length on the dipole moment. Rather, they have analyzed the dependence of the condensate properties on the *ratio* of the dipole moment to the scattering length. This is appropriate if one considers a fixed dipole moment (and scattering length) but varies the number of particles in the trap. On the other hand, the scenario we wish to consider is that where dipolar interactions are tuned by an external field, in which case the dipole moment and scattering length do not scale equally. Also, Ref. [12] did not consider negative dipole-dependent scattering lengths.

In this work we focus on a trapped gas of dipolar particles, where the interparticle interaction is dominated by the dipole-dipole force. A possible realization includes an (electrically polarized) gas of heteronuclear molecules with a large permanent electric dipole moment. The effective dipolar interaction may be tuned by the competition between an orienting electric field and the quantum or thermal rotation of the molecule. For example, the $^2\Pi_{3/2}$ ground state of the OH molecule is completely polarized in a field of about 10^4 V/cm. For smaller fields, the field strength determines the degree of polarization and the size of the dipole moment. Another approach for tuning the dipolar interaction, by using a rotating external field, was proposed in Ref. [19]. In the first approach, tuning the dipolar interaction by varying a static field is expected to affect the scattering length, as discussed below. However, in the approach of Ref. [19] the dipolar interaction is tuned through rotating the dipoles, and the time scale for the rotation is typically slower than that for two-body collisions in the gas. Therefore in this latter approach no effect on the scattering length is expected. In what follows we consider tuning by the first method, i.e., by a static external field.

We consider the case of a bare (zero dipole moment) positive scattering length, and show that as the dipole moment is increased, this scattering length becomes smaller and, above a certain dipole strength, negative, and then again positive after crossing a resonance. Taking this variation of the scattering length into account is necessary to describe the creation of new two-body bound states. This has consequences for the basic theory, and for the predicted stability of BECs with anisotropic interactions, especially for polar molecules,

*Electronic address: bohn@murphy.colorado.edu

which can have large dipole moments. To verify that the dipole-dependent scattering length is essential to reproducing the correct energetics, and to ascertain the validity of this approach, we have solved the many-body Schrödinger equation using the diffusion Monte Carlo (DMC) method, as well as solved the Schrödinger equation by direct diagonalization for two particles. In these calculations we used a potential consisting of short-range hard wall potential and long-range dipolar interaction. We then compare these results with solutions of the GPE, in which we employ the appropriate pseudopotential with the dipole-dependent scattering length.

Section II describes the system under study while Sec. III presents our results for dipolar gases under spherically symmetric and cylindrically symmetric confinement. Selected results for systems under spherically symmetric traps have been presented in a previous paper [20]. Here, we provide numerical details (see the Appendix), justify the formalism employed in detail, and significantly extend the discussion of our findings. Section IV concludes.

II. FORMULATION

For N identical bosons in an external trap potential $V_{\text{ext}}(\boldsymbol{r})$ with pairwise interaction $V(\boldsymbol{r}-\boldsymbol{r}')$, at zero temperature, the condensate is typically described using mean-field theory. All the particles in the condensate then have the same wave function $\psi(\boldsymbol{r})$. As a first attempt, one may write a Hartree-Fock equation for this wave function [21]

$$\mu\psi(\boldsymbol{r}) = \left[-\frac{\hbar^2}{2m}\nabla^2 + V_{\text{ext}}(\boldsymbol{r}) + (N-1) \times \int d\boldsymbol{r}'\, V(\boldsymbol{r}-\boldsymbol{r}')|\psi(\boldsymbol{r}')|^2 \right]\psi(\boldsymbol{r}), \tag{1}$$

where μ denotes the chemical potential, $\boldsymbol{r}$ the displacement from the trap center, and m the mass of a particle. In the following we restrict ourselves to cylindrically symmetric harmonic traps with $V_{\text{ext}}(\boldsymbol{r}) = \frac{1}{2}m(\omega_\rho^2\rho^2 + \omega_z^2 z^2)$.

We consider an interaction potential $V(\boldsymbol{r})$ which consists of a dipolar interaction and a short-range hard wall with cutoff radius b:

$$V(\boldsymbol{r}) = \begin{cases} d^2\dfrac{1-3\cos^2\theta}{r^3}, & \text{if } r \geqslant b, \\ \infty & \text{if } r < b, \end{cases} \tag{2}$$

where d denotes the dipole moment (in Gaussian units), r the distance vector between the dipoles, and θ the angle between the vector $\boldsymbol{r}$ and the dipole axis, which we take to be aligned along the $\hat{z}$ axis of the trap. The hardwall cutoff corresponds to hard particles with diameter b (two particles cannot penetrate each other when the distance between their centers is equal to their diameter). It is worth commenting on the validity of the mock potential (2) for describing realistic molecules. In general, at low energies only s-wave scattering is important, and a spherically symmetric hard wall potential is adequate. However, for polar molecules with a small λ doublet Δ_λ, there can be an effective long-range van der Waals coefficient $C_6^{\text{eff}} \propto d^2\Delta_\lambda$ that can be quite large [22]. If the temperature of the gas exceeds the height of the resulting d-wave centrifugal barrier, then even the short-range potential can exhibit an anisotropy, and a more elaborate short-range potential becomes necessary. To take an example, for the OH radical $C_6^{\text{eff}} \sim 4\times 10^4$ [22], which places this barrier at 1.6 mK, far above the temperature expected in BEC experiments.

Unfortunately, the short range part of the interaction potential V causes the integral in Eq. (1) to diverge. Fortunately, this divergence can be cured since the condensate is very dilute and ultracold, which implies that the particles in it are moving very slowly. Thus the potential V may be replaced by an effective potential (pseudopotential) V_{eff} with a milder small r behavior, which reproduces the two-body scattering wave function asymptotically in the zero energy limit, and which does not lead to divergences when used in the Hartree-Fock mean-field description.

For a short-range potential V, the low-energy scattering amplitude is completely determined by one parameter, the scattering length a, and an appropriate pseudopotential is $V_{\text{eff}}(\boldsymbol{r}) = \frac{4\pi\hbar^2 a}{m}\delta(\boldsymbol{r})$. In general, the pseudopotential is chosen such that its first-order Born scattering amplitude reproduces the complete scattering amplitude of the original potential V in the zero-energy limit. For a potential with long range dipolar part, Yi and You [11,12] proposed the following pseudopotential:

$$V_{\text{eff}}(\boldsymbol{r}) = \frac{4\pi\hbar^2 a(d)}{m}\delta(\boldsymbol{r}) + d^2\frac{1-3\cos^2\theta}{r^3}, \tag{3}$$

where the scattering length $a(d)$ depends on the dipole moment d. Note that the long-range part of the pseudopotential is identical to the long-range part of the original potential. By construction, the scattering amplitude of V_{eff} calculated in the first-order Born approximation agrees with the full zero-energy scattering amplitude of V. To verify the validity of the pseudopotential for systems of experimental interest, we compute the low energy scattering amplitude $f(\boldsymbol{k},\boldsymbol{k}')$ for two OH-like molecules interacting through the model potential given in Eq. (2), and compare it with the scattering amplitude computed in the first Born approximation.

The low-energy scattering amplitude in the presence of the long-range dipolar interaction may be expanded in partial waves

$$f(\boldsymbol{k},\boldsymbol{k}') = 4\pi \sum_{lm,l'm'} t_{lm}^{l'm'}(k) Y_{lm}^*(\hat{\boldsymbol{k}}) Y_{l'm'}(\hat{\boldsymbol{k}}'), \tag{4}$$

with the reduced T-matrix elements. The anisotropic dipolar potential implies that f depends on the incident and scattered directions $\hat{\boldsymbol{k}}$ and $\hat{\boldsymbol{k}}'$. The reduced T-matrix elements are related to the usual T-matrix elements $T_{lm}^{l'm'}(k) = \langle l'm'|\boldsymbol{T}(k)|lm\rangle$ by $t_{lm}^{l'm'}(k) = \frac{T_{lm}^{l'm'}(k)}{2k}$. For $k\to 0$ they are energy independent, and act as generalized scattering lengths. In particular, the scattering length $a(d)$ is given by $t_{00}^{00}(0)$ and depends on the dipole moment d.

Figure 1 compares some reduced T-matrix elements (symbols), computed through numerical close-coupling calculations, with the first Born approximation [11,12,23] (dashed

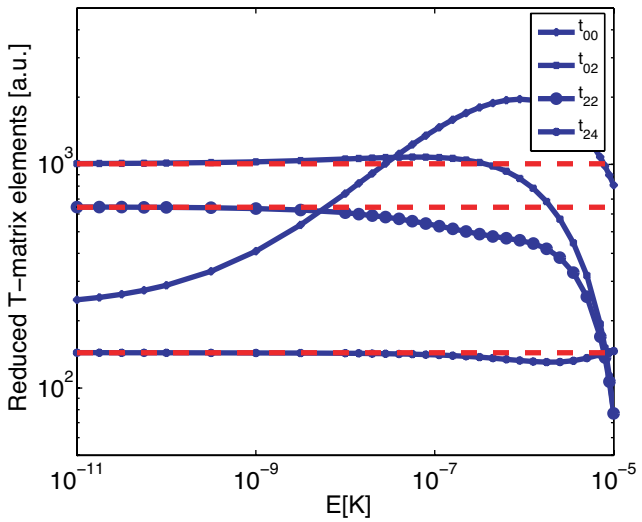

FIG. 1. (Color online) Absolute values of selected reduced T-matrix elements $t_{ll'} \equiv t_{l0}^{l'0}$ (symbols) for the OH-OH model potential as a function of the relative scattering energy, compared with the first-order Born approximation (dashed lines). Note, the first-order Born approximation to t_{00} diverges and is not shown.

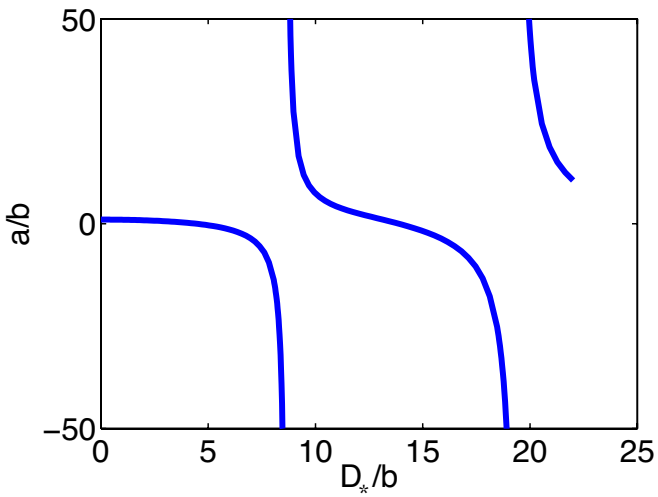

FIG. 2. (Color online) Scattering length $a(d)$ versus dipole length D_* for the dipolar potential with hard wall cutoff b given in Eq. (2).

lines), for the potential given in Eq. (2) with parameters chosen to describe the scattering between two rigid OH-like molecules. In particular, we have taken $m=17.00$ amu, $d=0.66$ a.u., and $b=105$ a.u. (this is a reasonable value for a molecular scattering length). For the t_{00}^{00} channel, the Born approximation to the long-range dipolar part of the potential gives no contribution, while that to the hardcore part diverges (and is therefore not shown in the figure). For the other channels, there is a remarkably good agreement in the $E\to 0$ limit between the exact reduced zero-energy T-matrix elements and those calculated in the first Born approximation. The agreement becomes less good at finite but small scattering energies (of the order 10^{-7} K). Also, $t_{00}^{00}(k)$ is not constant (as it would be in the threshold limit) even for very low energies of the order of 10^{-10} K. This suggests that, e.g., an effective range correction [24,25] may become important at finite E, but here we consider only the $E=0$ limit. The $t_{00}^{00}(k=0)$ matrix element determines $a(d)$, the dipole-dependent scattering length of the pseudopotential (3). In this way, the Born approximation to the pseudopotential gives the correct $t_{00}^{00}(k=0)$ value. The fact that $a(d)$ depends on d is important, since the strength of the dipolar interactions may be controlled by an external field. Our analysis confirms that the pseudopotential approximation provides a good description in regions away from resonance [11] (see also below).

Replacing V in Eq. (1) with V_{eff} of Eq. (3), with the scattering length $a(d)$ determined through numerical coupled-channel calculations for the model potential V, we obtain the (time-independent) Gross-Pitaevskii equation (GPE)

$$\mu\psi(\boldsymbol{r}) = \left[-\frac{\hbar^2}{2m}\nabla^2 + V_{\text{ext}}(\boldsymbol{r}) + (N-1)\right.$$
$$\left.\times \int d\boldsymbol{r}' V_{\text{eff}}(\boldsymbol{r}-\boldsymbol{r}')|\psi(\boldsymbol{r}')|^2\right]\psi(\boldsymbol{r}). \quad (5)$$

For the following, we define a dipole length $D_*=md^2/\hbar^2$. This is the distance at which the dipolar potential energy equals the kinetic energy (estimated from the uncertainty relation) of two interacting dipoles. In Fig. 2 we plot the ratio a/b of the scattering length a to the hardwall cutoff b as function of D_*/b. This provides a universal curve for the model potential given in Eq. (2), which determines the scattering length for any given cutoff b and dipole length D_*. Note the appearance of resonances, corresponding to the appearance of new bound states. In the neighborhood of a resonance, the scattering length tends towards $-\infty$ before and $+\infty$ after the resonance. These resonances have been identified before in dipolar scattering [11,26]. They would occur at fields of order MV/cm in atoms and kV/cm in heteronuclear molecules, or perhaps at 10^5 V/cm in atoms, if assisted by Feshbach resonances [27].

It is instructive to connect Fig. 2 back to concrete dipoles that can be handled in the laboratory. Consider, for example, atomic chromium, which is generating a lot of interest now that it has been Bose condensed. ^{52}Cr has a magnetic dipole moment of $6\mu_B$, and a sextet scattering length of 112 a.u. Identifying the hardwall cutoff with this scattering length, chromium would appear on Fig. 2 at the value $D_*/b=0.4$, and the scattering length would be renormalized by $\sim 0.6\%$ of its value in the absence of a dipole moment. Indeed, this correction is already included in two-body modeling of the Cr-Cr interaction [28,29]. For chromium, resonances of the type shown in Fig. 2 play no role. However, it may be possible to "turn off" the short-range interaction of Cr by means of a Feshbach resonance (in our toy model, this would correspond to taking the limit $b\to 0$). Shape resonances due to a dipolar bound Cr-Cr molecule might become accessible.

For a heteronuclear polar molecule, however, the situation can be quite different. Consider, for example, the OH radical, which is also the focus of intense experimental efforts [4,30]. This molecule has a permanent electric dipole moment of 0.66 atomic units, and therefore a huge dipole length $D_*=1.35\times 10^4$ a.u. If we assume a small cutoff, such as b

$=105$ a.u., then $D_*/b=128$, which is way off scale in Fig. 2. In other words, this potential supports a large number of OH-OH dimer states. These dimer states could play a large role in the physics of a gas composed of polar molecules.

III. MANY BODY AND TWO-BODY CALCULATIONS

The mean field GP approach to solving the many-body dynamics is necessarily approximate. However, the full N-body Schrödinger equation with the actual interaction potential V, Eq. (2), can be solved numerically for relatively small N. For $N=2$, the Schrödinger equation can be solved by direct diagonalization. For $N>2$, direct diagonalization becomes impractical and we solve the Schrödinger equation instead by the DMC method [31]. This section compares the results obtained by the three methods. Details of how these schemes are implemented are presented in the Appendix.

We note that the system is scalable: if the hardwall cutoff b and the dipole length D_* are each scaled by a factor K, then the scattering length scales by the same amount. If the harmonic oscillator lengths $\sqrt{\frac{\hbar}{m\omega_z}}$ and $\sqrt{\frac{\hbar}{m\omega_\rho}}$ are also scaled accordingly, then the entire spectrum (both the exact spectrum obtained by solving the N-body Schrödinger equation and the spectrum obtained within the mean field approximation) remains the same apart from scaling by a factor $1/K^2$.

In what follows, unless stated otherwise, we work with an isotropic harmonic trap $\omega_\rho=\omega_z\equiv\omega$. Correspondingly, the natural unit of length is the harmonic oscillator length $a_{\mathrm{HO}}=\sqrt{\frac{\hbar}{m\omega}}$. In the following, we consider the two-body potential V, Eq. (2), for two different values of b, i.e., $b=0.0137$ a.u. and $b=0.0433$ a.u., and varying d. For concreteness, OH molecules in a trap with a frequency $\omega=2\pi$ kHz would have $a_{\mathrm{HO}}=5800$ a.u. so that $b=0.0137a_{\mathrm{HO}}$ corresponds to a hardwall cutoff of 79 a.u.

A. Energies and collapse in an isotropic trap

In this paper, our primary interest is in BEC's of polar molecules. In such systems, the dipole moment is something that is directly under the experimentalist's control: in zero electric field the dipole moment vanishes, while at higher fields its value can be continuously tuned. For this reason, we consider properties of dipolar condensates as a function of the dipole moment, which is taken as a substitute for the dependence on the strength of an external electric field. One quantity can be converted into the other, of course, via the polarizability of the molecule.

Figure 3 presents the ground-state energy per particle in units of the harmonic oscillator energy $E_{\mathrm{HO}}=\hbar\omega$ versus the dipole length D_* in units of the harmonic oscillator length a_{HO} for $N=10$ molecules. In this figure, the solid line shows the GP energies obtained using V_{eff} with the dipole-dependent s-wave scattering length $a(d)$. For comparison, the symbols show the results from the DMC simulations, which solve the N-body Schrödinger equation for the model potential V, Eq. (2) (statistical uncertainties are indicated by vertical error bars). The agreement is excellent, attesting to the validity of parametrizing the GP equation in terms of the dipole-dependent scattering length $a(d)$.

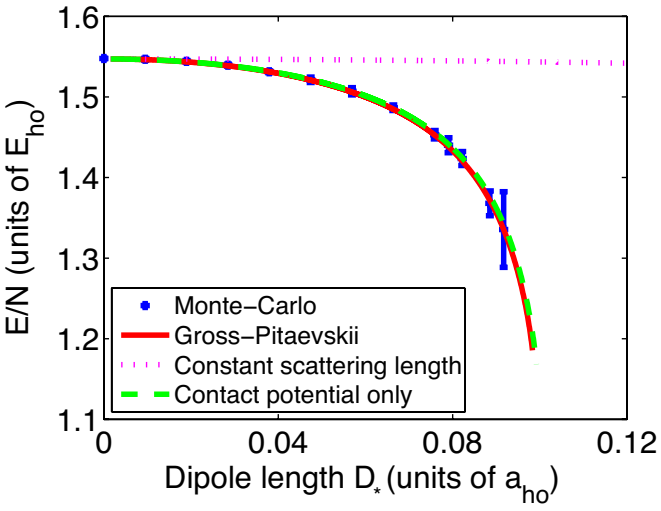

FIG. 3. (Color online) Energy per particle E/N as a function of the dipole length D_* for $N=10$. The symbols with error bars show DMC results. The solid line is the solution of the GPE. The dotted line shows a GP calculation without taking the dipole dependence of the scattering length into account, setting it equal to the hardwall cutoff. The dashed line shows a GP calculation with the dipole dependent scattering length, but omitting the long range dipolar term. The lines terminate at the collapse point of the condensate.

For zero dipole moment, the scattering length is equal to the hardwall cutoff b. Thus the energy per particle is larger than its noninteracting value of $1.5\hbar\omega$. As the dipole moment increases, the energy per particle drops. Qualitatively, this has been explained previously by an elongation of the dipolar gas in the z direction. This allows more dipoles to encounter one another in an attractive "head-to-tail" orientation. As shown below, we indeed observe an elongation of the condensate.

However, by far the greatest influence of the dipolar interaction on the condensate *energy* comes from the dipole dependent scattering length. To illustrate this, the dashed line in Fig. 3 shows the result of a GP calculation, which includes the contact (delta function) term of V_{eff} with the dipole dependent scattering length, but omits the nonisotropic dipolar long-range term. It is quite surprising how good this approximation is, in which the condensate is completely isotropic. For comparison, a dotted line shows the results from a GP calculation which keeps the long-range interaction, but does not take the dependence of the scattering length on the dipole moment into account. Instead, we use the zero-field scattering length, i.e., $a=b$. It is clear that this approximation greatly overestimates the energy. It is not even a very good approximation for small dipole moments [the second derivative at $d=0$ does not match the curvature for the "correct" GP solution (solid line)].

As the dipole moment increases, the condensate quickly moves toward a complete collapse, with $E/N\rightarrow-\infty$. This occurs because the scattering length attains a large, negative value. It is well known that a condensate with short range interaction only collapses when a critical combination of particle number and scattering length is reached, $(N-1)a=-0.57497a_{\mathrm{HO}}$ [32,33]. This is exactly the point

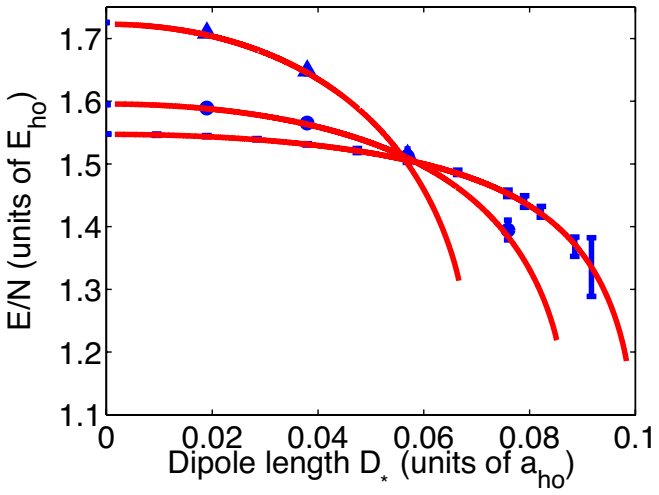

FIG. 4. (Color online) Energy per particle E/N as a function of the dipole length D_* for $N=10$, 20, and 50 (from top to bottom). Solid lines show mean field GP energies. Dots ($N=10$), circles ($N=20$), and triangles ($N=50$) show DMC energies. Error bars indicate the statistical uncertainties of the DMC energies.

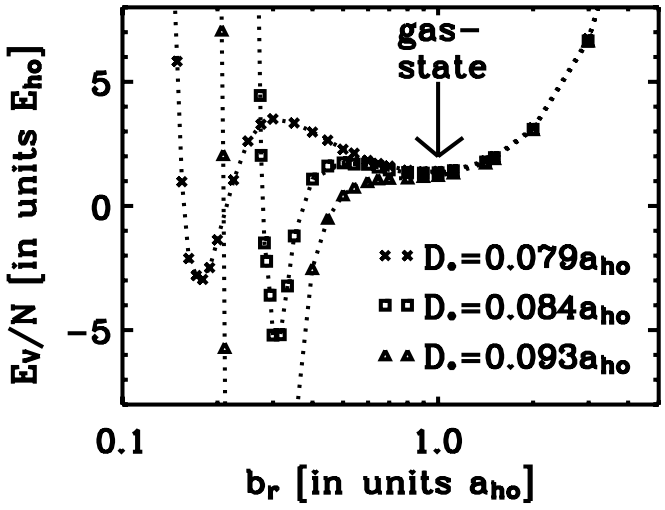

FIG. 5. Variational many-body energies E_V/N for $N=20$, $b=0.0137a_{\mathrm{HO}}$ and $D_*=0.079a_{\mathrm{HO}}$ (crosses), $D_*=0.084a_{\mathrm{HO}}$ (squares), and $D_*=0.093a_{\mathrm{HO}}$ (triangles) as a function of the Gaussian width b_r, where $b_r=b_\rho=b_z$.

where the dashed line in Fig. 3 terminates. It is also very nearly the point where the solid line, which provides the most complete description of dipolar gases at the GP level, terminates. The collapse discussed here is very different from that usually discussed in the context of dipolar gases, which takes the scattering length to be constant. In the latter case, collapse can also occur due to the presence of a large dipole moment, but (as seen from the dotted line in Fig. 3) this collapse occurs for much larger dipole moments than the value predicted here by taking the dependence of the scattering length on the dipole moment into account. We therefore predict a kind of electric-field-induced condensate collapse, which shares many similarities with the collapse encountered in alkali atom BEC's near magnetic field Feshbach resonances [33,34]. In particular, ramping the field across a resonance would likely result in the creation of dimer states of the molecules.

Figure 4 shows the dependence of the energy per particle on the dipole moment for various particle numbers $N=10$, 20, and 50. In all cases the conclusions are the same. Namely, the GP energies obtained using V_{eff} with the renormalized scattering length (solid lines) are an excellent approximation to the DMC energies (symbols). Also, the collapse occurs for smaller dipole moment as the particle number increases, in accord with the collapse criterion.

In the present discussion we have tuned the dipole moment starting from $d=0$. Because of the resonance structure shown in Fig. 2, it is possible to start with a large dipole moment and a small dipole-dependent scattering length. In this case we expect that the anisotropic long-range part of the effective potential will carry greater weight (i.e., will have a larger impact on the energetics and collapse). We have not considered this case in the present work.

We now investigate the stability of dipolar Bose gases by considering the variational energy E_V obtained by a variational many-body ansatz (see the Appendix for details and notation). Symbols in Fig. 5 show E_V/N for $b=0.0137a_{\mathrm{HO}}$, $N=20$ and three different values of D_*, i.e., $D_*=0.079a_{\mathrm{HO}}$ (crosses), $D_*=0.084a_{\mathrm{HO}}$ (squares), and $D_*=0.093a_{\mathrm{HO}}$ (triangles), as a function of the Gaussian width b_r, which is treated as a variational parameter (we set $b_\rho=b_z=b_r$ in this stability study). The variational parameters of F [Eq. (A6)] are optimized for $D_*=0.079a_{\mathrm{HO}}$ and $0.084a_{\mathrm{HO}}$ by minimizing the energy E_V for fixed b_ρ and b_z, i.e., for $b_\rho=b_z=1$. For $D_*=0.093a_{\mathrm{HO}}$, we use the same values for p_1 through p_5 as for $D_*=0.084a_{\mathrm{HO}}$ since no local minimum exists for $D_*=0.093a_{\mathrm{HO}}$ (see below).

Figure 5 indicates that the variational energy for $D_*=0.079a_{\mathrm{HO}}$ shows a local minimum at $b_r\approx 1a_{\mathrm{HO}}$ and a global minimum at $b_r\approx 0.09a_{\mathrm{HO}}$. The "barrier" at $b_r\approx 0.3a_{\mathrm{HO}}$ separates the large b_r region in configuration space, where the metastable condensate state exists, from the small b_r region where bound many-body states exist [43]. At very small b_r, the variational energy becomes large and positive due to the hardcore repulsion of the two-body potential. Figure 5 indicates that the energy barrier decreases with increasing D_*. The dipolar gas collapses at the D_*/a_{HO} value for which the energy barrier vanishes. Our DMC calculations show that the condensate prior to collapse is only slightly elongated, which justifies that our stability analysis parametrizes the one-body term ϕ [see Eq. (A5)] in terms of a single Gaussian width b_r and which is consistent with our finding that the collapse is induced primarily by the negative value of $a(d)$. We find similar results for other N values.

We emphasize that the presence of the energy barrier is crucial for our DMC calculations to converge to the metastable condensate state for sufficiently large D_*/a_{HO} and not to the clusterlike ground state (see also the Appendix).

B. Condensate sizes and shapes

The nature of the collapse is seen in more detail by looking at the size and shape of the condensate. To this end Fig.

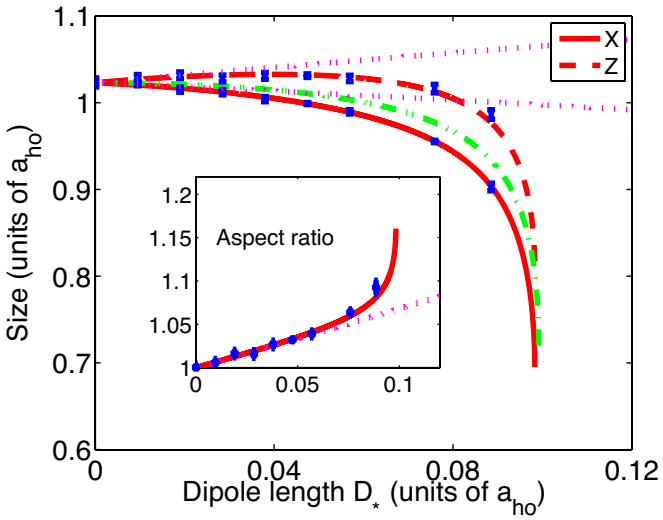

FIG. 6. (Color online) Condensate sizes $X=\sqrt{\langle x^2\rangle}$ and $Z=\sqrt{\langle z^2\rangle}$, for 10 particles with hard wall cutoff $b=0.0137a_{\mathrm{HO}}$ in a spherical trap. Solid and dashed lines show X and Z obtained by solving the GP equation using V_{eff} with the dipole-normalized scattering length. Symbols with error bars show the corresponding DMC results. The dotted lines show results of a GP calculation with constant scattering length $a=b$. The dash-dotted line shows results of a GP calculation with dipole dependent scattering length that omits the long range dipolar interaction. Inset: The aspect ratio Z/X for the solution to the GP equation using V_{eff} (solid line), for the solution to the GP equation with constant scattering length $a=b$ (dotted line), and for the DMC solution to the N-body Schrödinger equation (symbols with error bars).

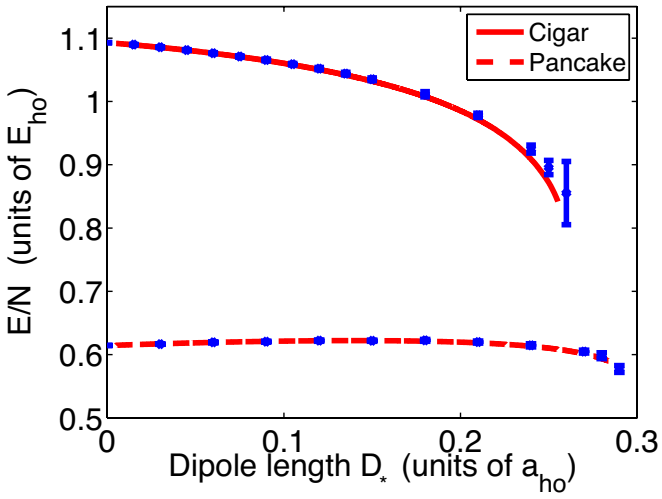

FIG. 7. (Color online) Energy per particle E/N obtained by solving the GP equation using V_{eff} as a function of the dipole length D_* for $N=10$ in a pancake-shaped trap with $\omega_z/\omega_\rho=10$ (dashed line) and in a cigar-shaped trap with $\omega_z/\omega_\rho=0.1$ (solid line). Symbols with error bars show the corresponding DMC results. a_{HO} is defined by the shortest dimension in each case (see text). The hard wall cutoff is $b=0.0137a_{\mathrm{HO}}$.

6 shows the root-mean-square widths Z and X of the condensate in the z and x directions, for $N=10$ and $b=0.0137a_{HO}$ (the same parameters as in Fig. 3). The solid and dashed lines are computed using the GP equation with the renormalized scattering length, and the symbols with error bars show, as before, the results of the DMC calculations; again, the agreement is excellent. For zero dipole moment, the condensate is isotropic and slightly larger than the harmonic oscillator length. As the dipole moment is turned on, the condensate contracts slightly in the x direction, and expands in the z direction. This illustrates the elongation that has been predicted for a dipolar condensate [12].

If in the effective potential we retain only the dipole-dependent scattering length, but omit the long-range dipolar term, we obtain the dash-dotted line. This approximation describes an isotropic condensate ($Z=X$) whose size is in between Z and X obtained by the more complete description (dashed and solid lines). On the other hand, if we retain the dipolar long-range term, but set the scattering length to a constant (its value for zero dipole moment, $a=b$), we obtain the dotted lines. This formulation overestimates the size of the condensate, but provides quite a good approximation to the aspect ratio Z/X (inset in Fig. 6)—at least for small dipole moments As the dipole moment is increased, the condensate approaches the point of collapse, and the aspect ratio calculated from the solution to the full GP equation (solid line in the inset) and the DMC calculations (symbols in the inset) increases rapidly. The approximation of a constant scattering length does not describe this behavior correctly. Interestingly, relatively large anisotropy is predicted just prior to collapse, even though the collapse mechanism is primarily s-wave dominated.

C. Energetics for dipoles in nonisotropic traps

We have also explored the behavior of dipolar BECs in a pancake-shaped trap with $\omega_z/\omega_\rho=10$ and in a cigar-shaped trap with $\omega_z/\omega_\rho=1/10$. For the pancake trap, we define $a_{\mathrm{HO}}=\sqrt{\frac{\hbar}{m\omega_z}}$, while for the cigar trap, $a_{\mathrm{HO}}=\sqrt{\frac{\hbar}{m\omega_\rho}}$. That is, compared to the spherical trap of the previous sections, we elongate the trap in either the axial or transverse directions. Figure 7 indicates very good agreement between the energies calculated from the GP equation (solid and dashed lines) and from the N-body Schrödinger equation (symbols). In the cigar-shaped trap, a nonvanishing dipole moment leads to a decrease of the energy compared to the energy obtained for $d=0$. For the pancake-shaped trap, in contrast, the energy per particle increases for small dipole moments, and then decreases for larger dipole moments. In both traps, collapse occurs at the D_* value at which the lines in Fig. 7 terminate.

We note in particular the collapse of the condensate in the pancake trap. In Ref. [16] it was proposed that in a trap of such aspect ratio, if the scattering length is zero, there should never be collapse even for an arbitrarily large dipole moment. In our case, the "bare" (zero dipole moment) scattering length is positive, and so, neglecting the scattering length dependence on the dipole moment, the BEC should be even more resistant to collapse. Later work [17], which analyzed dipolar BECs in a trap in the limit of $\omega_z/\omega_\rho=\infty$, suggests that a collapse should still occur even in highly elongated pancake traps, due to a roton-maxon instability involving excitations with large transverse momenta. As seen from Fig. 7

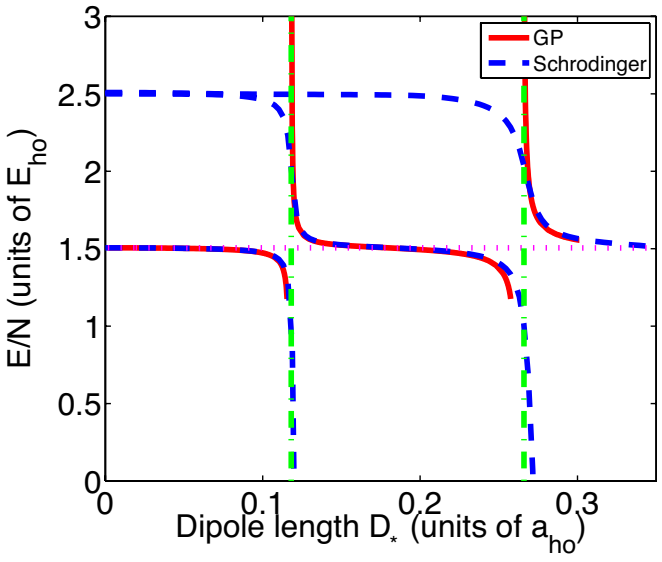

FIG. 8. (Color online) E/N for two particles with hard wall cutoff $b=0.0137a_{\mathrm{HO}}$ in a spherical trap as a function of the dipole length D_* obtained by solving the GP equation (solid lines) and the Schrödinger equation (dashed lines). The GP line terminates at points of collapse. For the Schrödinger equation, the three lowest eigenvalues are displayed (negative energies are not shown). The dotted line shows the results from a GP calculation with a constant scattering length $a=b$. The vertical dash-dotted lines indicate the resonance positions of V, Eq. (3) (see also Fig. 2).

we do observe a collapse of the condensate in the pancake trap, which, however, is due to the dependence of the scattering length on the dipole moment. This collapse mechanism is similar to that discussed above for spherical traps (see Fig. 3).

D. Excited states and condensate "revival"

The s-wave-dominated collapse shown in Fig. 3 does not necessarily signal the end of the story. After the scattering length has dropped to $-\infty$, it then takes on a large positive value (see Fig. 2). In this region, the condensate is, neglecting three-body recombination effects, perfectly stable, at least until the scattering length again becomes large and negative. As the resonance is crossed, a new two-body bound state appears in the potential (2). Indeed, this is the first bound state of this potential. In the following, we compare the energetics obtained by solving the GP equation and the Schrödinger equation for $N=2$ particles (see the Appendix) as the dipole moment is tuned across a series of two-body resonances. Extension of this analysis to more than $N=2$ particles is complicated by the existence of the two-body bound states of V, Eq. (2). These two-body bound states imply that solving the N-body Schrödinger equation by the DMC method requires the use of fixed-node techniques [35]. Such a treatment is beyond the scope of this paper.

Figure 8 shows E/N for two particles under spherically symmetric confinement with hardwall cutoff $b=0.0137a_{\mathrm{HO}}$. The exact two-body solution to the Schrödinger equation (dashed lines) shows a repeated cycle of collapse and "revival." For comparison, solid lines show the solution to the GP equation. In the regions away from resonance, Fig. 8 indicates good agreement between the GP energies and one of the "branches" of the exact two-body spectrum. To obtain this agreement, it is essential to use the dipole-normalized scattering length, which encapsulates the information about the formation of bound states of the system, in the effective potential that enters the GP equation. Otherwise, if a constant scattering length (corresponding to the zero dipole moment case with $a=b$) is used in the GP formalism, the unrealistic dotted line in Fig. 8 is obtained. This line can only be regarded as a good approximation in certain regions between resonances when the dipole dependent scattering length is small. As mentioned above, for computational reasons we have only performed this comparison for $N=2$, but it is strongly suggestive that the same should hold for any number of particles. By tuning the dipole moment, it should thus be possible to observe a collapse followed by a revival of a metastable dipolar BEC with increasing dipole strength. The results of a GP calculation for a stability diagram of a dipolar BEC as a function of the number of particles and the dipole moment is shown in Fig. 3 of Ref. [20].

In Fig. 8 the resonance positions from Fig. 2 for $b=0.0137a_{\mathrm{HO}}$ are indicated by vertical dash-dotted lines. The solution to the two-body Schrödinger equation persists to slightly larger dipole moments than the resonance position (this is most apparent for the second resonance), because of the added kinetic energy in the trap. By contrast, the GP solution collapses at a smaller dipole moment, owing to the approximate collapse criterion $(N-1)a(d)=-0.57497a_{\mathrm{HO}}$.

At this point we note that our solutions to the N-body Schrödinger equation have been restricted to relatively small number of particles ($N\leqslant 50$). It is sometimes asserted (see, e.g., Ref. [1]) that the GPE is valid only in the limit of large number of particles. This restriction comes from the derivation of the GPE from the exact Heisenberg representation equation, by replacing the Heisenberg field operator $\hat{\mathbf{\Psi}}(\boldsymbol{r})$ by its classical value $\mathbf{\Psi}_0(\boldsymbol{r})$. This breaks conservation of particle number, and can only be justified for a large number of particles. From this point of view, one might be surprised that the mean-field equation describes, as demonstrated here, systems with small number of particles with high accuracy. However, it is also possible to derive the GPE from a variational ansatz which explicitly conserves particle number [21,36]. This provides the justification for applying the GPE even for a small number of particles. In this case, it is important to keep the correct $N-1$ factor in Eq. (5), rather than, as is sometimes done, replace it by N, which can only be justified as an approximation valid for a large number of particles.

E. Limits of the mean field approximation

When the density of the condensate increases, one expects the mean field GP theory to become increasingly less accurate due to correlations among the particles. In the zero-dipole theory of short-range interactions the GP theory is the lowest order approximation in powers of the small parameter na^3, where n denotes the peak density and a the scattering

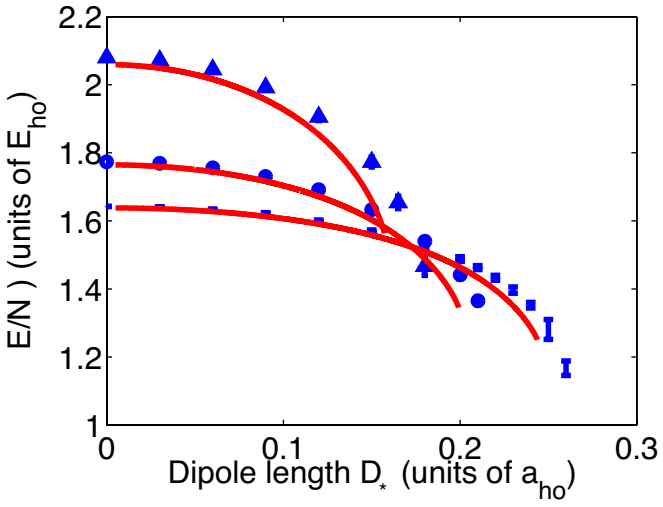

FIG. 9. (Color online) Energy per particle E/N versus dipole length D_* with hard-core radius $b=0.0433a_{\mathrm{HO}}$. Solid lines show the GP energies for $N=10$, 20, and 50 particles (from bottom to top). Symbols with error bars show the DMC energies for $N=10$ (dots), $N=20$ (circles), and $N=50$ (triangles).

length. The expansion parameter becomes larger as N and a increase. Treating larger number of particles in the DMC simulations increases the computational cost. Instead, to check the applicability of the GP theory to describe dense dipolar gases, we consider a larger particle diameter b. Figure 9 shows a comparison between the DMC energies (symbols with error bars) and the GP energies (solid lines) for $b=0.0433a_{\mathrm{HO}}$ which is a factor 3.2 larger than we considered in the previous sections. A good qualitative agreement still exists, but deviations are apparent. The GP calculations underestimate the many-body DMC energy, and the deviations grow with increasing number of particles N. The GP theory also predicts a collapse at a somewhat smaller d than the true value.

The deviations, which exist even for zero dipole moment, are attributed by us mainly to the relatively large hard core diameter $b=0.0433a_{\mathrm{HO}}$ of our "molecules" compared to the size of the trap. For zero dipole moment, such effects were observed before [37]. It was found that the deviations were reduced by roughly an order of magnitude by using a modified GPE that accounts for quantum fluctuations [38,39]. Even better agreement was achieved when effective range corrections were taken into account [25]. We expect that similar corrections would also apply to anisotropic dipolar gases. However, Ref. [37] described condensates with short-range repulsive interactions ($a>0$), for which the modified GPE included a correction term calculated in the local density approximation. In our case there is a long-range dipolar interaction which is partly attractive, and furthermore, the dipole dependent scattering length becomes negative for sufficiently large d. As a result, the local density approximation cannot be applied to our problem over the whole range, since a homogeneous condensate with attractive interactions is unstable.

Finally, we note that additional beyond mean-field corrections are expected to become important when the dipole length D_* becomes larger. Investigation of this regime is beyond the scope of this paper.

IV. CONCLUSIONS

In conclusion, we have considered a Bose gas with tunable dipolar interactions, controlled by an external field, and have shown that taking into account the dependence of the scattering length on the dipole moment is essential for the correct description of the system within the mean field GP method, using the pseudopotential of Yi and You [11]. By comparison with DMC simulations we have highlighted both the accuracy of the GP method for dipolar gases with low densities, and the existence of deviations for dipolar gases with higher densities. The mean field theory was shown to predict correctly the condensate size. It also describes well condensates in cylindrical and pancake traps. It was shown that as the dipole moment is increased, the scattering length decreases and becomes negative as one approaches a resonance corresponding to the formation of a two-body bound state. This effect is the major contribution for the eventual collapse of the condensate at a critical dipole moment. This is particularly significant for a pancake trap, in which case, failing to take the dependence of the scattering length on the dipole moment into account, collapse would occur only due to a roton-maxon instability. As the dipole moment is increased further, past the two-body resonance, the scattering length $a(d)$ becomes positive and we see a "revival" of a stable condensate.

ACKNOWLEDGMENTS

We thank T. Pfau for useful discussion. S.R. gratefully acknowledges financial support from an anonymous fund, and from the United States-Israel Educational Foundation (Fulbright Program), DCEB and JLB from the DOE and the Keck Foundation, and DB from the NSF under Grant No. PHY-0331529.

APPENDIX

In this Appendix we discuss the numerical techniques used in the three different methods of this paper: solution to the Gross-Pitaevskii equation, solution to the N-body Schrödinger equation by the DMC method, and solution to the two-body Schrödinger equation.

1. Solution of the Gross-Pitaevskii equation

Equation (5) with the pseudopotential Eq. (3) is an integrodifferential equation. The integral term $d^2\int d\boldsymbol{r}'\frac{1-3\cos^2\theta}{|\boldsymbol{r}-\boldsymbol{r}'|^3}|\psi(\boldsymbol{r}')|^2$ needs special attention due to the apparent divergence of the dipolar pseudopotential at small distances. The integral does converge if one performs the angular integration first. For small distances, the density $|\psi(\boldsymbol{r}')|^2$ may be considered linear around $\boldsymbol{r}'=\boldsymbol{r}$, and integrating the angular part with $Y_{20}\propto 1-3\cos^2\theta$ gives zero. This can also be seen by expanding the density in a multipole expansion around $\boldsymbol{r}'=\boldsymbol{r}$. Only the Y_{20} term will contribute to the inte-

gral, and for a smooth density the coefficient of this term goes, for $|\boldsymbol{r}-\boldsymbol{r}'|\to 0$, as $|\boldsymbol{r}-\boldsymbol{r}'|^2$. Thus, the integral converges even without a cutoff.

Following Ref. [13], the calculation of the integral can be simplified by means of the convolution theorem

$$\int d\boldsymbol{r}' V_D(\boldsymbol{r}-\boldsymbol{r}')|\psi(\boldsymbol{r}')|^2 = \mathcal{F}^{-1}\{\mathcal{F}[V_D](\boldsymbol{k})\mathcal{F}[|\psi|^2](\boldsymbol{k})\}, \tag{A1}$$

where $\mathcal{F}$ is the Fourier transform and V_D is the dipolar interaction part of V_{eff} of Eq. (3). The Fourier transform of the dipolar potential may be performed by expanding $\exp(i\boldsymbol{k}\cdot\boldsymbol{r})$ in a series of spherical harmonics and spherical Bessel functions (the usual expansion of a free planar wave in free spherical waves), where only the Y_{20} term gives a nonzero contribution. The result is

$$\mathcal{F}[V_D](\boldsymbol{k}) = d^2\frac{4\pi}{3}(3\cos^2\alpha - 1), \tag{A2}$$

where α is the angle between the momentum $\boldsymbol{k}$ and the dipole direction. The Fourier transform of Eq. (A1), $\mathcal{F}(|\psi|^2)$ is numerically evaluated by means of a standard fast Fourier transform (FFT) algorithm, and multiplied by $\mathcal{F}[V_D](\boldsymbol{k})$. Computation of the kinetic energy is also accomplished to spectral accuracy through a FFT of the wave function and multiplication by k^2 in momentum space, followed by an inverse FFT.

The ground state of the system was obtained by the usual wave-function propagation in imaginary time. The propagation was implemented using a fourth order adaptive step Runge-Kutta method.

This procedure is very computationally intensive. We have recently developed an improved method, which we also partly used in this work, and which we describe elsewhere.

2. Diffusion Monte Carlo simulations

The many-body Hamiltonian H for a dipolar gas under external confinement reads

$$H = \sum_{j=1}^{N}\left[-\frac{\hbar^2}{2m}\nabla_j^2 + \frac{1}{2}m(\omega_\rho^2\rho_j^2 + \omega_z^2 z_j^2)\right] + \sum_{j<k} V(r_{jk},\theta_{jk}), \tag{A3}$$

where V denotes the interaction potential given by Eq. (2), $\boldsymbol{r}_j=(x_j,y_j,z_j)$ the position vector of the jth dipole, $\boldsymbol{r}_{jk}$ the distance vector, i.e., $\boldsymbol{r}_{jk}=\boldsymbol{r}_j-\boldsymbol{r}_k$, and θ_{jk} the angle between the vector $\boldsymbol{r}_{jk}$ and the z axis. To solve the corresponding time-independent Schrödinger equation $H\psi=E\psi$ we employ the variational Monte Carlo (VMC) and the diffusion Monte Carlo (DMC) techniques [31]. The former results in a variational bound on the energy whereas the latter results in essentially exact many-body energies.

To determine variational many-body energies, we write the variational wave function ψ_V as a product of one-body terms ϕ and two-body terms F,

$$\psi_V(\boldsymbol{r}_1,\ldots,\boldsymbol{r}_N) = \prod_{j=1}^{N}\phi(\rho_j,z_j)\prod_{j<k}^{N}F(r_{jk},\theta_{jk}), \tag{A4}$$

where ϕ contains the Gaussian widths b_ρ and b_z,

$$\phi(\rho,z) = \exp\left[-\frac{1}{2}\left(\frac{\rho}{b_\rho}\right)^2 - \frac{1}{2}\left(\frac{z}{b_z}\right)^2\right], \tag{A5}$$

and F the hardcore radius b and the "shape" parameters p_1-p_5,

$$F(r,\theta) = \left[1-\frac{b}{r}\right]\left[1+\frac{1}{r^{p_3}}(p_1+p_2\cos^2\theta)+\frac{p_4}{r^{p_5}}\cos^4\theta\right]. \tag{A6}$$

To first order the parameters of ϕ are determined by the external confining potential and those of F by the two-body potential V. For a noninteracting gas with $b=d=0$, e.g., the variational wave function ψ_V with $b_\rho=b_z=1$ and $p_1=p_2=p_4=0$ is an exact solution to the many-body Schrödinger equation. For a finite hardcore radius b, the term in the first pair of square brackets on the right hand side of Eq. (A6) coincides with the low-energy s-wave scattering wave function for two particles interacting through a spherically symmetric hardcore potential with radius b, i.e., this term ensures that the many-body wave function goes to zero as the distance r between two particles approaches the hardcore radius b. The functional form of the angle-dependent term of F [term in the second pair of square brackets on the right-hand side of Eq. (A6)] is motivated by the shape of the essentially exact two-body wave functions for nonvanishing d^2, which is obtained numerically using B splines (see Sec. 3 in the Appendix).

The variational parameters b_ρ, b_z, and p_1-p_5, collectively denoted by $\boldsymbol{p}$, are optimized for each N, ω_ρ, ω_z, and D_* by minimizing the energy E_V,

$$E_V(\boldsymbol{p}) = \frac{\langle\psi_V(\boldsymbol{p})|H|\psi_V(\boldsymbol{p})\rangle}{\langle\psi_V(\boldsymbol{p})|\psi_V(\boldsymbol{p})\rangle}, \tag{A7}$$

where the integration over the $3N$ coordinates $\boldsymbol{r}_1,\ldots,\boldsymbol{r}_N$ is performed using Metropolis sampling. Our parametrization of the variational wave function ψ_V provides an excellent description of weakly interacting gases with small nb^3 and nD_*^3, where n denotes the condensate density at the trap center. As b/a_{HO} or D_*/a_{HO} increase, i.e., as the gas becomes more strongly interacting, the VMC energy E_V recovers an increasingly smaller fraction of the essentially exact DMC energy.

The optimized variational wave function ψ_V is subsequently used as a guiding function in our DMC calculations with importance sampling. The DMC technique solves the many-body Schrödinger equation for the ground state energy and for structural properties by starting with an initial "walker distribution," which can be thought of as a stochastic representation of the many-body wave function, and by then projecting out the lowest stationary eigenstate through propagation in imaginary time. To treat high-dimensional systems (here with as many as 150 degrees of freedom), the short-time Green's function propagator is evaluated stochas-

tically. The resulting DMC energies are essentially exact, i.e., they are independent of ψ_V, with the only uncertainty stemming from the finite time step used in the propagation. For the DMC energies reported, the time step errors are smaller than the statistical uncertainties. Usage of a good guiding function, i.e., our optimized ψ_V, is essential for the DMC algorithm to be numerically stable. If ψ_V coincides with the exact many-body wave function—as is the case for noninteracting inhomogeneous gases—the resulting DMC energies have vanishing variance and thus vanishing error bars. Interactions, and correspondingly approximate ψ_V, introduce statistical uncertainties in the DMC energies, which can be reduced by increasing the computational efforts. We calculate structural expectation values using a descendant weighting scheme [40–42], which in principle eliminates any dependence of the structural expectation values on ψ_V. However, our structural expectation values may be slightly biased by ψ_V since there is a tradeoff between the statistical uncertainty and the lengths of the "side walks" used in the descendant weighting scheme.

The standard DMC algorithm outlined above describes the ground state. To describe metastable condensates, i.e., excited many-body states with gaslike character, our DMC simulations take advantage of the topology of the underlying configuration space. The metastable condensate state, characterized by large interparticle distances, is separated from bound many-body states, characterized by small interparticle distances, by a "barrier" (see Sec. III A). In this respect, the topology of the high-dimensional configuration space at hand is similar to the configuration space of a one-dimensional double-well potential with large barrier. For large enough barrier, the two regions in configuration space correspond to two effectively orthogonal Hilbert spaces. This implies that DMC walkers with initial coordinates corresponding to a metastable gaslike state have a vanishingly small probability to tunnel into the region of configuration space corresponding to molecularlike bound states and that the simulations consequently converge to the metastable condensate state and not to energetically lower-lying cluster states. The presence of the barrier is thus crucial for describing metastable condensate states with negative scattering length by the DMC algorithm.

3. Numerical solution of Schrödinger equation for two dipoles

For two dipoles in a trap interacting through the potential of Eq. (2), the Schrödinger equation is separable in relative distance and center-of-mass coordinates. The center of mass equation describes the harmonic motion of the two dipoles as a whole in the trap, and has the usual harmonic oscillator ground state. The relative distance equation has cylindrical symmetry and was solved numerically by expanding the wave function on a basis set of two-dimensional B splines, with the appropriate boundary conditions. The full Hamiltonian matrix in this basis was constructed and diagonalized.

[1] L. P. Pitaevskii and S. Stringari, *Bose-Einstein Condensation* (Oxford University Press, New York, 2003).
[2] F. Dalfovo, S. Giorgini, L. P. Pitaevskii, and S. Stringari, Rev. Mod. Phys. **71**, 463 (1999).
[3] J. Doyle, B. Friedrich, R. V. Krems, and F. Masnou-Seeuws, Eur. Phys. J. D **31**, 149 (2004).
[4] J. M. Sage, S. Sainis, T. Bergeman, and D. DeMille, Phys. Rev. Lett. **94**, 203001 (2005).
[5] C. A. Stan, M. W. Zwierlein, C. H. Schunck, S. M. F. Raupach, and W. Ketterle, Phys. Rev. Lett. **93**, 143001 (2004).
[6] S. Inouye, J. Goldwin, M. L. Olsen, C. Ticknor, J. L. Bohn, and D. S. Jin, Phys. Rev. Lett. **93**, 183201 (2004).
[7] A. Simoni, F. Ferlaino, G. Roati, G. Modugno, and M. Inguscio, Phys. Rev. Lett. **90**, 163202 (2003).
[8] S. Y. T. van de Meerakker, P. H. M. Smeets, N. Vanhaecke, R. T. Jongma, and G. Meijer, Phys. Rev. Lett. **94**, 023004 (2005).
[9] J. Stuhler, A. Griesmaier, T. Koch, M. Fattori, T. Pfau, S. Giovanazzi, P. Pedri, and L. Santos, Phys. Rev. Lett. **95**, 150406 (2005).
[10] K. Góral, K. Rzążewski, and T. Pfau, Phys. Rev. A **61**, 051601(R) (2000).
[11] S. Yi and L. You, Phys. Rev. A **61**, 041604(R) (2000).
[12] S. Yi and L. You, Phys. Rev. A **63**, 053607 (2001).
[13] K. Góral and L. Santos, Phys. Rev. A **66**, 023613 (2002).
[14] M. Baranov, L. Dobrek, K. Góral, L. Santos, and M. Lewenstein, Phys. Scr. **T102**, 74 (2002).
[15] D. H. J. O'Dell, S. Giovanazzi, and C. Eberlein, Phys. Rev. Lett. **92**, 250401 (2004).
[16] L. Santos, G. V. Shlyapnikov, P. Zoller, and M. Lewenstein, Phys. Rev. Lett. **85**, 1791 (2000).
[17] L. Santos, G. V. Shlyapnikov, and M. Lewenstein, Phys. Rev. Lett. **90**, 250403 (2003).
[18] K. Nho and D. P. Landau, Phys. Rev. A **72**, 023615 (2005).
[19] S. Giovanazzi, A. Görlitz, and T. Pfau, Phys. Rev. Lett. **89**, 130401 (2002).
[20] D. C. E. Bortolotti, S. Ronen, J. L. Bohn, and D. Blume, cond-mat/0604432 (unpublished).
[21] B. D. Esry, Phys. Rev. A **55**, 1147 (1997).
[22] A. V. Avdeenkov and J. L. Bohn, Phys. Rev. A **66**, 052718 (2005).
[23] A. V. Avdeenkov and J. L. Bohn, Phys. Rev. A **71**, 022706 (2005).
[24] E. Braaten, H. W. Hammer, and S. Hermans, Phys. Rev. A **63**, 063609 (2001).
[25] H. Fu, Y. Wang, and B. Gao, Phys. Rev. A **67**, 053612 (2003).
[26] C. Ticknor and J. L. Bohn, Phys. Rev. A **72**, 032717 (2005).
[27] R. V. Krems, Phys. Rev. Lett. **96**, 123202 (2006).
[28] J. Werner, A. Griesmaier, S. Hensler, J. Stuhler, T. Pfau, A. Simoni, and E. Tiesinga, Phys. Rev. Lett. **94**, 183201 (2005).
[29] Z. Pavlović, R. V. Krems, R. Côté, and H. R. Sadeghpour, Phys. Rev. A **71**, 061402(R) (2005).
[30] J. R. Bochinski, E. R. Hudson, H. J. Lewandowski, and J. Ye, Phys. Rev. A **70**, 043410 (2004).
[31] B. L. Hammond, W. A. Lester, Jr., and P. J. Reynolds, *Monte*

Carlo Methods in Ab Initio Quantum Chemistry (World Scientific, Singapore, 1994).
[32] R. J. Dodd, M. Edwards, C. J. Williams, C. W. Clark, M. J. Holland, P. A. Ruprecht, and K. Burnett, Phys. Rev. A **54**, 661 (1996).
[33] C. C. Bradley, C. A. Sackett, and R. G. Hulet, Phys. Rev. Lett. **78**, 985 (1997).
[34] E. A. Donley, N. R. Claussen, S. L. Cornish, J. L. Roberts, E. A. Cornell, and C. E. Wieman, Nature (London) **412**, 295 (2001).
[35] P. J. Reynolds, D. M. Ceperley, B. J. Alder, and W. A. Lester, Jr., J. Chem. Phys. **77**, 5593 (1982).
[36] A. J. Leggett, Rev. Mod. Phys. **73**, 307 (2001).
[37] D. Blume and C. H. Greene, Phys. Rev. A **63**, 063601 (2001).
[38] E. Braaten and A. Nieto, Phys. Rev. B **56**, 14745 (1997).
[39] E. Timmermans, P. Tommasini, and K. Huang, Phys. Rev. A **55**, 3645 (1997).
[40] M. H. Kalos, D. Levesque, and L. Verlet, Phys. Rev. A **9**, 2178 (1974).
[41] K. S. Liu, M. H. Kalos, and G. V. Chester, Phys. Rev. A **10**, 303 (1974).
[42] R. N. Barnett, P. J. Reynolds, and W. A. Lester, Jr., J. Comput. Phys. **96**, 258 (1991).
[43] Many-body bound states exist for sufficiently large D_*/a_{HO} even though the two-body potential used in our DMC calculations does not support any bound states.